Research Article | Vol. 9, No. 8 | 1 Aug 2018 | BIOMEDICAL OPTICS EXPRESS 3534
Biomedical Optics EXPRESS

Comparing the effective attenuation lengths for long wavelength *in vivo* imaging of the mouse brain

MENGRAN WANG,* CHUNYAN WU, DAVID SINEFELD, BO LI, FEI XIA, AND CHRIS XU

School of Applied and Engineering Physics, Cornell University, Ithaca, NY 14853, USA
mw827@cornell.edu

Abstract: Light attenuation in thick biological tissues, caused by a combination of absorption and scattering, limits the penetration depth in multiphoton microscopy (MPM). Both tissue scattering and absorption are dependent on wavelengths, which makes it essential to choose the excitation wavelength with minimum attenuation for deep imaging. Although theoretical models have been established to predict the wavelength dependence of light attenuation in brain tissues, the accuracy of these models in experimental settings needs to be verified. Furthermore, the water absorption contribution to the tissue attenuation, especially at 1450 nm where strong water absorption is predicted to be the dominant contributor in light attenuation, has not been confirmed. Here we performed a systematic study of *in vivo* three-photon imaging at different excitation wavelengths, 1300 nm, 1450 nm, 1500 nm, 1550 nm, and 1700 nm, and quantified the tissue attenuation by calculating the effective attenuation length at each wavelength. The experimental data show that the effective attenuation length at 1450 nm is significantly shorter than that at 1300 nm or 1700 nm. Our results provide unequivocal validation of the theoretical estimations based on water absorption and tissue scattering in predicting the effective attenuation lengths for long wavelength *in vivo* imaging.

OCIS codes: (180.4315) Nonlinear microscopy; (170.3880) Medical and biological imaging.

References and links

1. W. Denk, J. H. Strickler, and W. W. Webb, "Two-photon laser scanning fluorescence microscopy," Science **248**, 73–76 (1990).
2. W. Denk and K. Svoboda, "Photon upmanship: Why multiphoton imaging is more than a gimmick," Neuron **18**, 351–357 (1997).
3. N. G. Horton, K. Wang, D. Kobat, C. G. Clark, F. W. Wise, C. B. Schaffer, and C. Xu, "*In vivo* three-photon microscopy of subcortical structures within an intact mouse brain," Nat. Photonics **7**, 205–209 (2013).
4. D. G. Ouzounov, T. Wang, M. Wang, D. D. Feng, N. G. Horton, J. C. Cruz-Hernández, Y.-T. Cheng, J. Reimer, A. S. Tolias, N. Nishimura, and C. Xu, "*In vivo* three-photon imaging of activity of GCaMP6-labeled neurons deep in intact mouse brain," Nat. Methods **14**, 388–390 (2017).
5. J. Ying, F. Liu, and R. R. Alfano, "Effect of scattering on nonlinear optical scanning microscopy imaging of highly scattering media," Appl. Opt. **39**, 509–514 (2000).
6. A. K. Dunn, V. P. Wallace, M. Coleno, M. W. Berns, and B. J. Tromberg, "Influence of optical properties on two-photon fluorescence imaging in turbid samples," Appl. Opt. **39**, 1194–1201 (2000).
7. M. Oheim, E. Beaurepaire, E. Chaigneau, J. Mertz, and S. Charpak, "Two-photon microscopy in brain tissue: parameters influencing the imaging depth," J. Neurosci. Methods **111**, 29–37 (2001).
8. F. Helmchen and W. Denk, "Deep tissue two-photon microscopy," Nat. Methods **2**, 932–940 (2005).
9. A. Roggan, M. Friebel, K. Doerschel, A. Hahn, and G. J. Mueller, "Optical properties of circulating human blood in the wavelength range 400–2500 nm," J. Biomed. Opt **4**, 36–47 (1999).
10. M. Friebel, A. Roggan, G. J. Müller, and M. C. Meinke, "Determination of optical properties of human blood in the spectral range 250 to 1100 nm using Monte Carlo simulations with hematocrit-dependent effective scattering phase functions," J. Biomed. Opt **11**, 034021 (2006).
11. S. L. Jacques, "Optical properties of biological tissues: a review," Phys. Med. Biol. **58**, R37 (2013).
12. R. F. Reinoso, B. A. Telfer, and M. Rowland, "Tissue water content in rats measured by desiccation," J. Pharmacol. Toxicol. Methods **38**, 87–92 (1997).
13. L. Kou, "Refractive indices of water and ice in the 0.65- to 2.5-μm spectral range," Appl. Opt. **32**, 3531–3540 (1993).

#331233 https://doi.org/10.1364/BOE.9.003534
Journal © 2018 Received 9 May 2018; revised 13 Jun 2018; accepted 20 Jun 2018; published 5 Jul 2018

Biomedical Optics EXPRESS

14. P. Theer, M. T. Hasan, and W. Denk, "Two-photon imaging to a depth of 1000 μm in living brains by use of a Ti:Al_2O_3 regenerative amplifier," Opt. Lett. **28**, 1022–1024 (2003).
15. W. F. Cheong, S. A. Prahl, and A. J. Welch, "A review of the optical properties of biological tissues," IEEE J. Quantum Electron. **26**, 2166–2185 (1990).
16. K. Wang, N. G. Horton, K. Charan, and C. Xu, "Advanced fiber soliton sources for nonlinear deep tissue imaging in biophotonics," IEEE J. Sel. Top. Quantum Electron. **20**, 50–60 (2014).
17. D. Kobat, M. E. Durst, N. Nishimura, A. W. Wong, C. B. Schaffer, and C. Xu, "Deep tissue multiphoton microscopy using longer wavelength excitation," Opt. Express **17**, 13354–13364 (2009).
18. T. Wang, D. Ouzounov, M. Wang, and C. Xu, "Quantitative Comparison of Two-photon and Three-photon Activity Imaging of GCaMP6s-labeled Neurons *in vivo* in the Mouse Brain," in "Optics in the Life Sciences Congress (2017)," (Optical Society of America, 2017), p. BrM4B.4.
19. M. Balu, "Effect of excitation wavelength on penetration depth in nonlinear optical microscopy of turbid media," J. Biomed. Opt. **14**, 010508 (2009).
20. V. J. Srinivasan, H. Radhakrishnan, J. Y. Jiang, S. Barry, and A. E. Cable, "Optical coherence microscopy for deep tissue imaging of the cerebral cortex with intrinsic contrast," Opt. Express **20**, 2220–2239 (2012).
21. D. Kobat, N. G. Horton, and C. Xu, "*In vivo* two-photon microscopy to 1.6-mm depth in mouse cortex," J. Biomed. Opt **16**, 106014 (2011).
22. S. P. Chong, C. W. Merkle, D. F. Cooke, T. Zhang, H. Radhakrishnan, L. Krubitzer, and V. J. Srinivasan, "Noninvasive, *in vivo* imaging of subcortical mouse brain regions with 1.7 μm optical coherence tomography," Opt. Lett. **40**, 4911–4914 (2015).
23. A. Zoumi, A. Yeh, and B. J. Tromberg, "Imaging cells and extracellular matrix *in vivo* by using second-harmonic generation and two-photon excited fluorescence," Proc. Natl. Acad. Sci. **99**, 11014–11019 (2002).
24. D. Kleinfeld, P. P. Mitra, F. Helmchen, and W. Denk, "Fluctuations and stimulus-induced changes in blood flow observed in individual capillaries in layers 2 through 4 of rat neocortex," Proc. Natl. Acad. Sci. **95**, 15741–15746 (1998).
25. *Two-photon imaging of neocortical microcirculation, booktitle = Imaging Neurons: A Laboratory Manual, publisher = Cold Spring Harbor Laboratory Press, author = Kleinfeld, David and Denk, Winfried, year = 1999, pages = 23.1–23.15*.
26. K. Charan, B. Li, M. Wang, C. P. Lin, and C. Xu, "Fiber-based tunable repetition rate source for deep tissue two-photon fluorescence microscopy," Biomed. Opt. Express **9**, 2304–2311 (2018).
27. N. G. Horton and C. Xu, "Dispersion compensation in three-photon fluorescence microscopy at 1,700 nm," Biomed. Opt. Express **6**, 1392–1397 (2015).
28. K. Wang, R. Liang, and P. Qiu, "Fluorescence Signal Generation Optimization by Optimal Filling of the High Numerical Aperture Objective Lens for High-Order Deep-Tissue Multiphoton Fluorescence Microscopy," IEEE Photonics J. **7**, 1–8 (2015).
29. C. Xu and W. W. Webb, *Multiphoton Excitation of Molecular Fluorophores and Nonlinear Laser Microscopy*, vol. 5 (Springer, 1997).
30. T.-W. Chen, T. J. Wardill, Y. Sun, S. R. Pulver, S. L. Renninger, A. Baohan, E. R. Schreiter, R. A. Kerr, M. B. Orger, V. Jayaraman, L. L. Looger, K. Svoboda, and D. S. Kim, "Ultrasensitive fluorescent proteins for imaging neuronal activity," Nature. **499**, 295–300 (2013).
31. H. Dana, B. Mohar, Y. Sun, S. Narayan, A. Gordus, J. P. Hasseman, G. Tsegaye, G. T. Holt, A. Hu, D. Walpita, R. Patel, J. J. Macklin, C. I. Bargmann, M. B. Ahrens, E. R. Schreiter, V. Jayaraman, L. L. Looger, K. Svoboda, and D. S. Kim, "Sensitive red protein calcium indicators for imaging neural activity," eLife. **5**, e12727 (2016).

1. Introduction

Multiphoton microscopy (MPM) enables deep imaging in highly scattering biological tissues due to the use of nonlinear excitation and long excitation wavelengths [1–4]. It has been demonstrated that the multiphoton excited fluorescence signal within the focal volume is mostly generated by ballistic photons (photons that maintain their ballistic trajectories). When imaging deep in scattering biological samples such as the mouse brain, the number of ballistic photons arriving at the focus is significantly reduced due to the absorption and scattering by the tissue [5, 6], characterized by the effective attenuation length (EAL). The ballistic photons as a function of depth (z) can be expressed as:

$$P_z = P_0 e^{-\frac{z}{l_e}}. \tag{1}$$

where P_z is the optical power at the focus, P_0 is the optical power on the sample surface, and l_e is the EAL.

The loss of ballistic photons reduces the fluorescence generation. In order to obtain sufficient signal from the focus, the exponential decay of the excitation light needs to be compensated by

Biomedical Optics EXPRESS

increasing the total optical power at the surface. Obviously, with the same excitation power, less tissue attenuation (or longer EAL) will allow for deeper tissue penetration [7].

Light attenuation in biological tissues is a combined effect of absorption and scattering. Using mouse brain tissue *in vivo* as an example, at wavelengths between 700 nm and 1060 nm—the wavelength tuning range of the mode-locked Ti:S laser—attenuation of the excitation light is completely dominated by tissue scattering [8], while the absorption (mostly by blood for *in vivo* imaging) is relatively low [9–11]. Longer wavelengths at approximately 1200 nm–1850 nm are advantageous for deep brain imaging due to the reduction of light scattering. However, water absorption (water content is >70% in brain tissues [12]) increases significantly in this spectral region and becomes the dominant absorber for *in vivo* imaging. Both water absorption and tissue scattering contribute to the attenuation of the excitation light, therefore, the optimum choice of the excitation wavelength is a trade-off between these two factors. The theoretical model of calculating l_e (Fig. 1) is then [3]:

$$\frac{1}{l_e} = \frac{1}{l_a} + \frac{1}{l_s}. \tag{2}$$

where l_a is the water absorption length [13], and l_s is the scattering mean-free path, calculated using Mie scattering for a tissue-like colloidal solution containing 1-μm diameter beads at a concentration of 5.4x10^9 beads/mL [14–16].

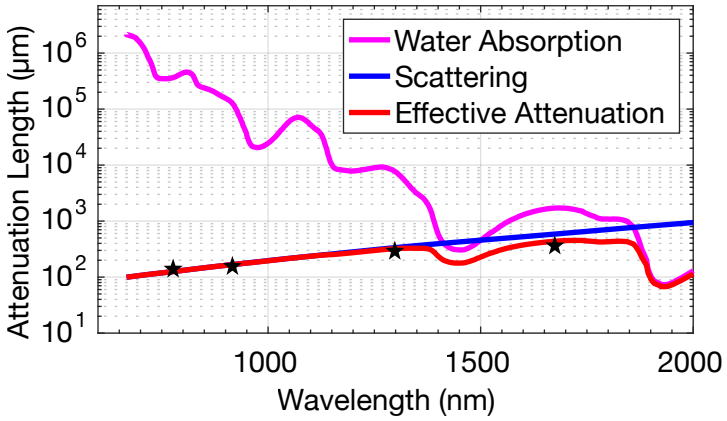

Fig. 1. Theoretical model of the effective attenuation lengths based on water absorption and Mie scattering. The black stars indicate the reported effective attenuation lengths in mouse brains *in vivo*, 131 μm at 775 nm [17], 152~158 μm at 920 nm [18], 305~319 μm at 1300 nm [18] and 383 μm at 1680 nm [3].

Theoretical estimations based on tissue absorption and scattering predict that the longer excitation wavelength approach is advantageous for deeper tissue imaging (Fig. 1), and previous experimental works have shown that the longer wavelength windows of 1300 nm [17–22] and 1700 nm [3, 22] outperform the shorter wavelengths, such as 775 nm [17], 800 nm [19, 23], 830 nm [24, 25], 920 nm [14, 18, 26], by a factor of 2 to 3 times in terms of imaging depth. However, the attenuation at these wavelengths are all dominated by scattering (i.e., l_a is at least several times larger than l_s). As previous experimental data all lie close to the scattering curve (the blue line in Fig. 1), it indicates that scattering alone, without any consideration of the absorption, would have predicted similar wavelength dependence. In particular, the absorption-scattering model predicts that the long wavelength window is not one continuous window. Instead, it indicates that there are two windows for mouse brain imaging centered at ~ 1300 nm and 1700 nm, with a gap at ~ 1450 nm due to strong water absorption (Fig. 1). In this paper, we compared

Biomedical Optics EXPRESS

the effective attenuation lengths at the excitation wavelengths of 1300 nm, 1450 nm, 1500 nm, 1550 nm, and 1700 nm in mouse brains *in vivo*. Our results confirm the existence of the water absorption feature in the wavelength dependence of EAL, and provide unequivocal support for the absorption-scattering model for ballistic photon penetration.

2. Characterization of the excitation source at 1700 nm, 1550 nm, 1500 nm, and 1450 nm

The three-photon imaging setup is similar to that described previously [3, 4]. The excitation source was a wavelength-tunable optical parametric amplifier (OPA, Opera-F, Coherent) pumped by a Monaco amplifier (Coherent) operating at 330 kHz repetition rate. The excitation pulse spectra at 1700 nm, 1550 nm, 1500 nm, and 1450 nm were measured by an Optical Spectrum Analyzer (OSA, Thorlabs), shown in Fig. 2(a).

We measured the dependence of the fluorescence from Texas Red on the excitation power at 1700 nm and 1450 nm to ensure three-photon excitation (Figs. 2(b) and 2(c)). The generated fluorescence was detected by a photomultiplier tube (PMT) with a GaAsP photocathode (H7422-40, Hamamatsu Photonics), and recorded by a photon counter (SR400, Stanford Research Systems). The slopes in the log-log plots confirmed three-photon excitation for Texas Red at both 1700 nm and 1450 nm.

Dispersion from the optics in the microscope were pre-compensated using a Si wafer (Edmund Optics) placed at the Brewster angle [27]. Second-order interferometric autocorrelations were performed after the objective lens at each wavelength (Fig. 3).

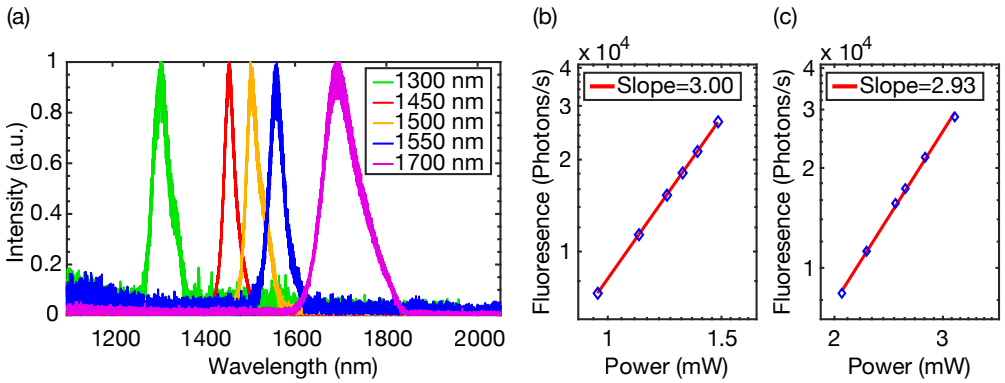

Fig. 2. (a) Measured spectra of the laser source operating at 1700 nm, 1550 nm, 1500 nm, 1450 nm and 1300 nm. Dependence of three-photon-excited fluorescence on excitation power for (b) 1700 nm and (c) 1450 nm in logarithmic scales. The blue diamonds are the measured data, and the red lines are linear fits to the experimental results. The slope is indicated in each figure.

The excitation beam size at the back aperture of the objective lens impacts the measurements of the EALs, since the marginal rays have longer path lengths in the tissue and experience more attenuation than the chief rays at the center of the lens. To ensure there is no systematic bias in the EAL measurements, we characterized the beam size at each excitation wavelength (Fig. 4) using a calibrated InGaAs camera (Axiom Optics, WiDy SWIR 640). The measurements were taken before the scanner and there is a 6x magnification from the scan mirrors to the back aperture of the objective lens. The beam size variation at these wavelengths is below 6%, which has negligible impact on the EAL measurements [28].

Biomedical Optics EXPRESS

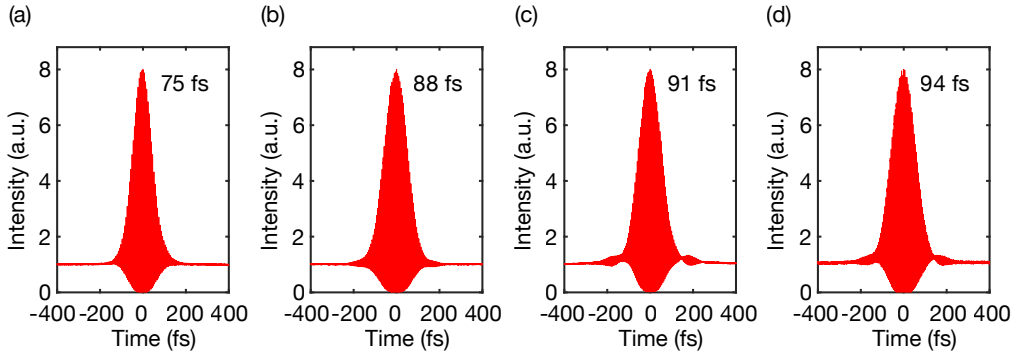

Fig. 3. Measured second-order interferometric autocorrelations of the laser pulse operating at (a) 1700 nm, (b) 1550 nm, (c) 1500 nm, and (d) 1450 nm. The intensity full-width-at-half-maximum (FWHM) of the pulse is indicated in each figure, assuming a deconvolution factor of 1.54 for sech^2-pulse.

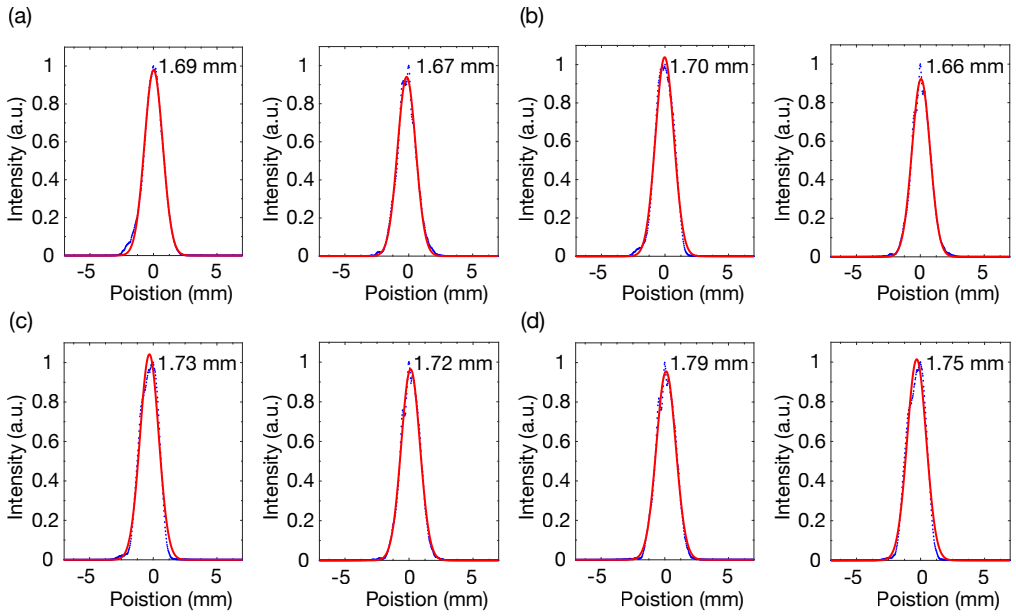

Fig. 4. Beam size measurements at (a) 1700 nm, (b) 1550 nm, (c) 1500 nm, and (d) 1450 nm. The blue dots are the measured data, and the red lines are Gaussian fits to the measurements. There is some ellipticity in the excitation beam, therefore the measurements were taken along both the long axis (left) and the short axis (right). The FWHM is labeled in each figure.

3. *In vivo* EAL measurements at 1700 nm, 1550 nm, 1500 nm, and 1450 nm excitation wavelengths

A craniotomy was performed on a 10-week-old wild-type mouse (C57BL/6J) and a glass window was placed directly on the intact dura for imaging. The mouse was anesthetized using isoflurane (3% in oxygen for induction and 1.5–2% for surgery and imaging to maintain a breathing frequency of 1 Hz). Body temperature was kept at 37.5 °C with a feedback-controlled blanket (Harvard Apparatus), and eye ointment was applied. Dextran-conjugated Texas Red (70kDa, Invitrogen) was injected retro-orbitally for the brain vasculature labeling prior to imaging.

Biomedical Optics EXPRESS

Three-photon imaging was performed in the same intact brain using four different excitation wavelengths, in the order of 1700 nm, 1550 nm, 1500 nm, 1450 nm, and 1700 nm. The 1700 nm excitation was repeated again at the end of the imaging session to ensure that the imaging sequence did not impact the measurements. All imaging were done using the same fluorophore in the same brain regions within the same mouse, which eliminated the uncertainty caused by the emission-wavelength difference and tissue-to-tissue variation. All images were taken at a frame rate of 0.24 Hz (512 x 512 pixels/frame) with a field of view (FOV) of 340 x 340 μm, and 10 frames were averaged at each depth. The detection path was kept the same for all the wavelengths in this comparison. Thus, the differences in the EALs were only due to the different excitation wavelengths used.

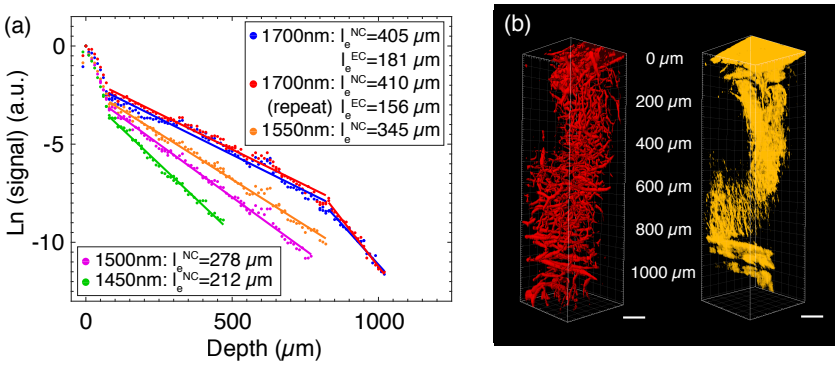

Fig. 5. (a) Comparison of the fluorescence signal as a function of depth at 1700 nm, 1550 nm, 1500 nm, 1450 nm, and 1700 nm (repeat experiment). The dots are the measured data, and the lines are linear fits to the measurements. With the same maximum average power, imaging at 1700 nm excitation includes both the neocortex (NC) and external capsule (EC), while imaging using the other wavelengths is limited to the NC. (b) 3D reconstruction of three-photon images of Texas Red-labeled brain vasculature, left, fluorescence, right, third harmonic generation (THG). Imaging depths are labeled in the middle. Scale bars, 100 μm.

We acquired approximately 1-mm-deep z-stack, taken at 10-μm depth increment. To avoid potential tissue heating, especially at 1450 nm due to the high water absorption, we kept the maximum average power on the brain surface at 35 mW for all the excitation wavelengths used. Power curves (dependence of the signal value on excitation power) were measured to ensure that no fluorophore saturation (i.e., ground state depletion) occurred at any imaging depth.

The fluorescence signal generated in three-photon microscopy (F_{3P}) is proportional to power cubic [29]. Combining Eq. (1), we have:

$$F_{3P} \propto P_z^3 = P_0^3 e^{-\frac{3z}{l_e}}. \tag{3}$$

We selected the average value of the brightest 1% of pixels in the x-y image at each depth as the fluorescence signal. In three-photon microscopy (3PM), EAL is defined as the depth at which the normalized signal attenuates by $1/e^3$. By plotting the fluorescence signal as a function of depth, the EALs can be obtained from the slopes of the linear fits in Fig. 5(a) for the neocortex (NC, 0–840 μm) and the external capsule (EC, 840–1040 μm), assuming the vasculature was labeled homogenously throughout the imaging regions. Measured EALs in the NC at different wavelengths with an uncertainty estimation based on the 95% confidence interval (CI) are: 391~418 μm at 1700 nm, 337~353 μm at 1550 nm, 272~283 μm at 1500 nm, 207~218 μm at 1450 nm, and 398~422 μm at 1700 nm (repeat experiment).

Biomedical Optics EXPRESS

To ensure that the results are not dependent on the selection criteria for the brightest pixels, we varied the selection criteria, and found that this variation did not affect the EAL measurements significantly. Taking the neocortex images acquired at 1700 nm as an example, we selected 0.5% (l_e=400 μm, 386~414 μm with 95% CI), 1% (l_e=405 μm, 391~418 μm with 95% CI), 1.5% (l_e=408 μm, 394~423 μm with 95% CI) and 2% (l_e=410 μm, 396~426 μm with 95% CI) of the brightest pixels. With all the selection criteria between 0.5% and 2%, the resulting EALs vary by ~ 2.5%, which will have no impact on the conclusion of this paper.

We also reconstructed the images from all depths for both fluorescence signal and third harmonic generation (THG) signal. The dense myelin layer in the external capsule (EC) generates strong THG, which allows us to delineate the neocortex and the external capsule (Fig. 5(b)). Although blood is assumed to be homogeneously distributed within the brain region, the presence of a large blood vessel at the brain surface (see Fig. 6(a)) results in the steeper slope at the beginning of each decay curve (Fig. 5(a), 0–80 μm). Since the brightest pixels are all within this large vessel, the fluorescence signal decays rapidly, reflecting the fact that the attenuation length for blood is much shorter than that of the brain tissue. The measured EALs within this large vessel (0–80 μm, top 1% brightest pixels represented as signal) are: 117 μm at 1700 nm (97~137 μm with 95% CI), 89 μm at 1550 nm (80~98 μm with 95% CI), 81 μm at 1500 nm (76~87 μm with 95% CI), 68 μm at 1450 nm (65~72 μm with 95% CI), and 112 μm at 1700 nm (repeat experiment, 88~136 μm with 95% CI).

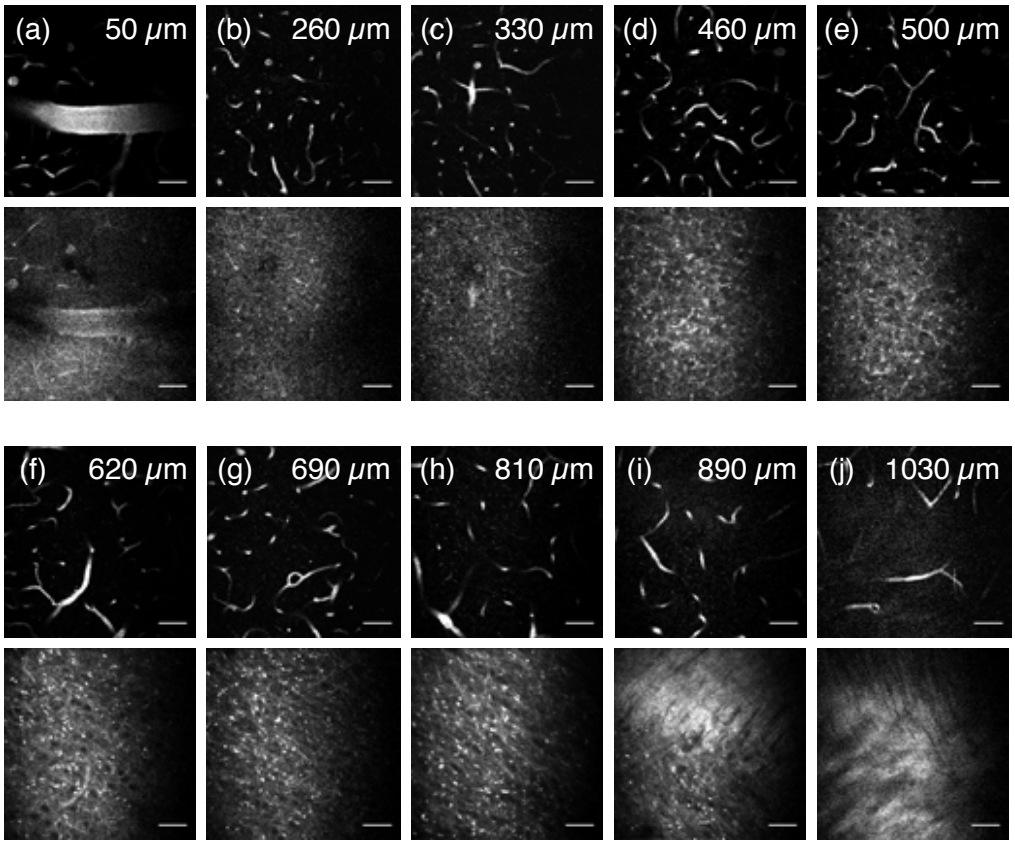

Fig. 6. Three-photon fluorescence images of the brain vasculature (upper) and THG images (lower) using 1700 nm excitation. The depths are indicated in the images. All the images are shown with the same contrast setting with the brightest 1% pixels saturated. Scale bars, 50 μm.

Biomedical Optics EXPRESS

Similar measurements were repeated on different mice. The absolute EAL values varied somewhat among the different mice, which could be caused by variations in the surgical preparation or the individuality of the mice. Nonetheless, the relative trend of the EALs, i.e., l_e (1700 nm) > l_e (1550 nm) > l_e (1500 nm) > l_e (1450 nm), holds for all the mice. Three of them are listed in Table 1.

Table 1. Summary of *in vivo* EAL measurements of the neocortex (NC) in three mice

Mouse	1700 nm	1550 nm	1500 nm	1450 nm	1700 nm (repeat)
Mouse1	405 μm	319 μm	278 μm	212 μm	410 μm
Mouse 2	350 μm	257 μm	220 μm	173 μm	348 μm
Mouse 3	370 μm	283 μm	241 μm	188 μm	370 μm

4. *In vivo* EAL measurements at 1300 nm and 1450 nm excitation wavelengths

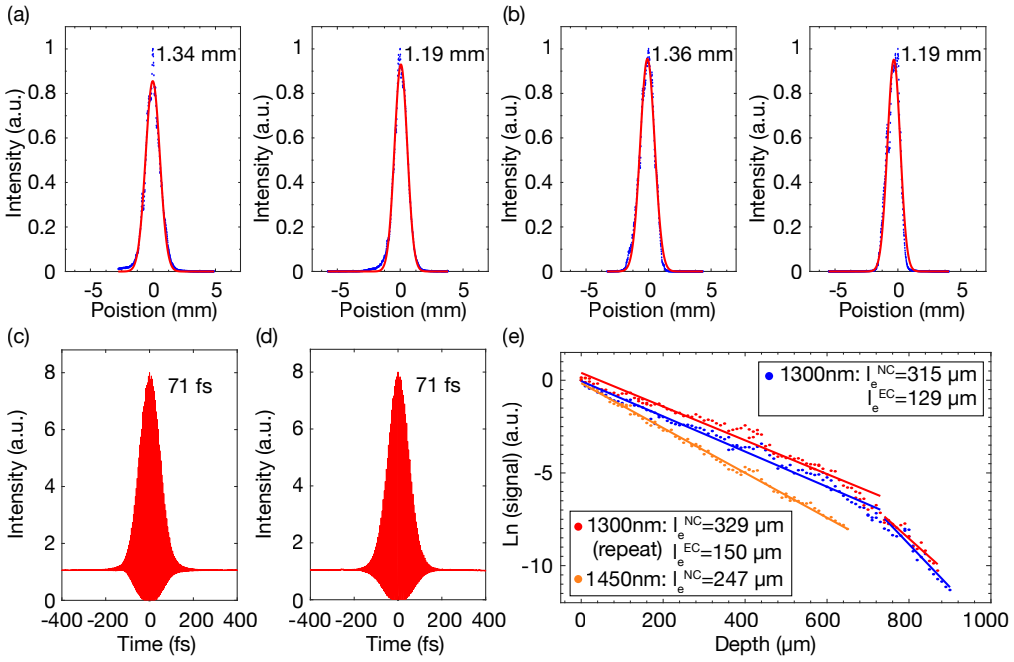

Fig. 7. Beam size measurements at (a) 1300 nm and (b) 1450 nm. The blue dots are the measured data, and the red lines are Gaussian fits to the measurements. Measurements were taken along both the long axis (left) and the short axis (right). The FWHM is labeled in each figure. Measured second-order interferometric autocorrelations of the laser pulse operating at (c) 1300 nm and (d) 1450 nm. The FWHM of the pulse is indicated in the figure, assuming a deconvolution factor of 1.54 for sech^2-pulse. (e) Comparison of the fluorescence signal as a function of depth at 1300 nm, 1450 nm, and 1300 nm (repeat experiment). The dots are the measured data, and the lines are linear fits to the measurements. With the same maximum average power, imaging by 1300 nm excitation includes both the NC and EC, while imaging by 1450 nm is limited to the NC.

In order to verify the contribution of water absorption in tissue attenuation at 1450 nm, we performed an additional comparison experiment of EAL measurements at 1300 nm and 1450 nm excitation wavelengths. The laser spectra at 1300 nm and 1450 nm are shown in Fig. 2(a). The

Biomedical Optics EXPRESS

beam sizes at both excitation wavelengths were measured before the scanner (Figs. 7(a) and 7(b)), with differences less than 1.5%. Second-order interferometric autocorrelations were performed after the objective lens at both wavelengths (Figs. 7(c) and 7(d)). The characterization method was the same as described in Section 2.

Because a mixture of 2- and 3-photon fluorescence from Texas Red is generated at 1300 nm excitation, we carried out this experiment separately using Fluorescein. Three-photon imaging was performed on the same Fluorescein-labeled (dextran conjugate, 70kDa, Invitrogen) vasculature in an intact mouse brain *in vivo* in the order of 1300 nm, 1450 nm and 1300 nm (as a repeat). The results are presented in Fig. 7(e) for the neocortex (NC, 0–740 μm) and the external capsule (EC, 740–900 μm). Measured EALs in the NC at different wavelengths with 95% CI are: 304~326 μm at 1300 nm, 243~251 μm at 1450 nm, 315~345 μm at 1300 nm (repeat experiment). The results at 1300 nm are consistent with previous studies [17, 18, 21] and are longer than that at 1450 nm. This comparison confirmed that water absorption is a key factor in the tissue attenuation at 1450 nm.

5. Discussion

The average values of the EAL measurements at different wavelengths are plotted together with the theoretical prediction (Fig. 8), indicating a close match between the experiments and theory.

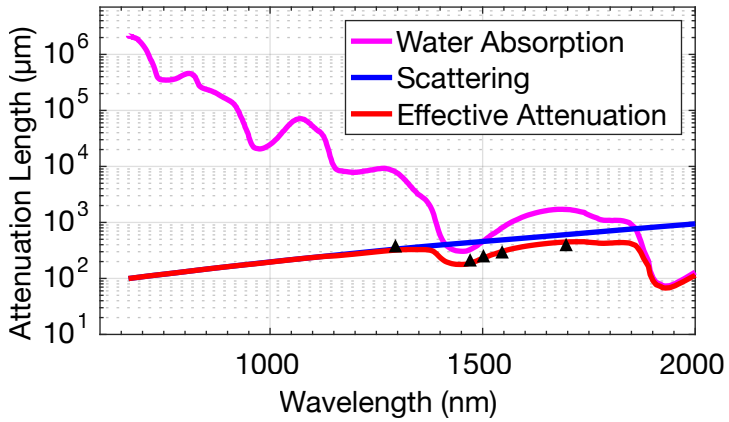

Fig. 8. Experimental data (averaged from all the measured EALs for each wavelength, black triangles) is shown on the same plot together with the theoretical model, indicating the accuracy of the model at predicting the experimental measurements at these excitation wavelengths.

Measurements of the EAL can be influenced by the excitation beam characteristics. The excitation beam in the experiments with fluorescein is somewhat different (e.g., beam diameter) from that with Texas Red, making the comparison of the EALs at 1450 nm obtained by the imaging results based on Texas Red and Fluorescein difficult. Even more important, there can be variations in the tissue properties or animal preparations (e.g., cranial window implant) when different mice are used. For example, the EALs for three different mice varied by approximately 20% in our measurements at 1450 nm (Table 1), even with the same beam characteristics and the same fluorophore.

Our comparison results confirm that there is less light attenuation at 1300 nm and 1700 nm than at 1450 nm. Although 1300 nm and 1700 nm are optimum in the long wavelength window for *in vivo* deep tissue multiphoton imaging, the selection between 1300 nm and 1700 nm depends on the imaging applications. There is more tissue attenuation (shorter EAL) at 1300 nm excitation than

Biomedical Optics EXPRESS

at 1700 nm; however, 1300 nm has less tissue absorption, which allows for higher excitation power at the brain surface. It is therefore a trade-off between the coefficient (P_0) and the exponent (l_e) in Eq. (1), 1300 nm will be the wavelength of choice for relatively shallow regions and 1700 nm will perform better for pushing the absolute imaging depth, especially when the signal-to-background ratio (SBR) is also taken into account [8]. Estimations based on the measured EALs and the permissible average power show that 1300 nm is more appropriate for imaging in the neocortex, while 1700 nm is perhaps more advantageous for imaging subcortical regions. In addition, the choice of the excitation wavelength certainly depends on the fluorophores. For brain activity imaging, for example, the robust, green fluorescent protein (GFP) based genetically encoded calcium indicators (GECIs) such as GCaMPs [30] dictate the use of 1300 nm excitation, while red fluorescent GECIs (RCaMPs, RGECOs [31]) would require the use of 1700 nm excitation.

6. Conclusion

We performed a systematic study of the impact of different excitation wavelengths on multiphoton imaging of the mouse brain *in vivo*. By comparing the effective attenuation lengths at 1300 nm, 1450 nm, 1500 nm, 1550 nm, and 1700 nm excitation wavelengths, we experimentally verified the water absorption contribution in brain tissue attenuation, especially at 1450 nm. Our results show that the theoretical estimations based on water absorption and tissue scattering are accurate in predicting tissue attenuation in the long wavelength window. This study can be used as an experimental guide of selecting excitation wavelengths for mouse brain imaging applications. For MPM of mouse brain *in vivo*, the spectral windows of 1300 nm and 1700 nm are optimum for deep imaging.

Funding

National Science Foundation (DBI-1707312); Department of Interior/Interior Business Center (DoI/IBC) (D16PC00003).

Acknowledgments

This work is supported by NSF DBI-1707312 NeuroNex grant, and supported by the Intelligence Advanced Research Projects Activity (IARPA) via Department of Interior/Interior Business Center (DoI/IBC) contract number D16PC00003.

The U.S. Government is authorized to reproduce and distribute reprints for Governmental purposes notwithstanding any copyright annotation thereon. Disclaimer: The views and conclusions contained herein are those of the authors and should not be interpreted as necessarily representing the official policies or endorsements, either expressed or implied, of IARPA, DoI/IBC, or the U.S. Government.

Disclosures

The authors declare that there are no conflicts of interest related to this article.